Towards sustainable rechargeable batteries via Single Point Exposure Laser Powder Bed Fusion of pure Zn lattice structures

L. Caprio[1], C. Baldi[1], E. Emanuele[2], B. Bozzini[2], B. Previtali[1], A.G. Demir[1]

[1]Department of Mechanical Engineering, Politecnico di Milano, Via La Masa 1, 20156, Milano, Italy
[2]Department of Energy, Politecnico di Milano, Via Lambruschini 4, 20156, Milano, Italy

Abstract

Rechargeable Zn-based batteries are highly promising sustainable post-lithium electrochemical energy storage technologies. Pure Zn is the active material of choice, but its cyclability is impaired by a range of morphochemical issues, namely dendrite growth, surface passivation and hydrogen formation. Diverse surface modification and structuring approaches on Zn anodes based on thin sheets have been proposed in the literature, to mitigate such issues. Laser Powder Bed Fusion (LPBF) is an ~~so far~~ unexplored route to anode engineering. Single Point Exposure (SPE) strategy can open up further potentialities for the formation of complex electrode architectures with tuned porosity. In this work we describe manufacturing of porous Zn anodes based on strut lattices using a dedicated LPBF system with accurate control of the laser temporal emission profile. A comprehensive set of samples was characterized in terms of their physical (apparent density, roughness and thickness) and electrochemical characteristics, disclosing the influence of process parameters on their activity and stability as battery electrodes.

Keywords: Laser Powder Bed Fusion, Zinc, Batteries, Anode

Introduction

With the ongoing transition towards a sustainable and circular economy, there is a strong requirement for the development of recyclable and low carbon footprint energy storage solutions. From this perspective rechargeable Zn-based batteries possess favourable characteristics and may eventually pose an alternative to the current Li-based systems [1,2]. Zinc intrinsically exhibits beneficial aspects with respect to Lithium including the possibility of a two-electron transfer as opposed to one, high material availability and elevated recyclability of the base material [3]. Moreover, from a safety perspective Zn-air or aqueous Zn batteries are naturally favoured with respect to Li-based systems that require organic electrolytes which are highly flammable and generate hydrofluoric acid when exposed to humid air.

Nonetheless, in order to develop secondary zinc batteries with high performance there are several issues that still need to be overcome. For instance, surface passivation phenomena may hinder the rechargeability of Zn-based batteries [4]. Dendrite formation on the anode during battery cycling is another aspect which can generate issues, since it can pierce the separator between anode and cathode thus causing short-circuiting of the battery[5]. Moreover, Hydrogen Evolution Reaction (HER) tends to occur in such conditions which is an undesirable effect, since it decreases energy density, it consumes the electrolyte and can interrupt the ionic contact, owing to bubble formation [6]. All of these aspects are currently being tackled within the scientific community and there is evidence that novel anode architectures obtainable through advanced production methods may enable the realisation of functional secondary Zn-based batteries. Zinc anodes with increased surface area and controlled permeability can be achieved using advanced production techniques paving the way to secondary batteries. For instance, Parker *et al.* showed that pure Zn anodes with three dimensional geometrical structures (as opposed to conventional laminated foils) exhibit promising behaviour for the development of such energy storage solutions considering their capability of inhibiting dendrite formation during charge-discharge cycling[7]. Further research demonstrated that Zn-Ni batteries possess energy density characteristics compatible to the current status of Li-ion solutions[8]. The fundamental aspect enabling the performance of the electrodes was their inherent 3D

sponge-like structure which was obtained by combining Zn powder with a polymer binder. Tian *et al.* used the direct ink writing (DIW) technique to deposit Zn-based electrodes [9]. From this perspective, the use of powder bed fusion additive manufacturing techniques offers an appealing solution given the capability of the process of consolidating metallic powders without the addition of a non-conductive binder which inherently impacts over the electro-chemical capabilities of the system. As a matter of fact, there is evidence that such technology may be employed to realise anodes with both architectured or process-induced stochastic porosities. Complex lattice structures with different levels of porosity may be digitally designed and realised through LPBF[10]. On the other hand, by exploiting keyhole induced or lack-of-fusion pores it is possible to design permeable structures[11]. Examples of such use can be found in regenerative fuel cells [12].

Nonetheless, laser powder bed fusion of Zn and its alloys is a challenging process given rapid tendency to evaporate of zinc when irradiated by a laser beam. Montani *et al.* and Demir *et al.* were amongst the first to experiment this approach for the deposition of pure Zn for biodegradable implants[13,14]. Chen *et al.* explored the use of strong fume extraction in order to suppress vapour formation[15]. Baldi *et al.* began exploring this technique at single track level and showcased the first examples of thin-walled structures for energy storage applications [16]. The use of novel beam shaping approaches was also investigated by modifying the spatial emission profile of the laser beam from Gaussian to ring-mode producing thin walls with stochastic surface structures due to the presence of partially remolten particles [16]. Although this solution demonstrates an indirect control over the surface geometry and porosity, the use of lattice structures with designed complex and intricate geometries is highly appealing for a greater control over the battery behaviour. Analogously, within the field of biomedical applications, zinc lattice structures with deterministic porosity produced by LPBF are widely studied. Li *et al.* showcased the applicability of architectured porous zinc structures for biodegradable implants demonstrating their biocompatibility and mechanical properties [17]. Similarly, Cockerill *et al.* investigated the use of zinc for the realisation of porous scaffolds [18]. Zn-based alloys have also been explored in order to tailor the mechanical and corrosion properties of the material[19]. Recently, Guaglione *et al.* exploited single point exposure (SPE) for the deposition of BCC-based lattice structures producing fine struts while largely suppressing the smoke and spatter generation [20,21]. Single point exposure relies on a different processing mechanism of the powder bed, with respect to the conventional raster-scan approach. In fact, in the case of SPE, the beam is exposed in a stationary way for a given time period over the metallic feedstock, thus generating a rounded melt region that can be exploited to construct the struts in a layerwise fashion exploiting the highest process resolution. From this perspective, it stands out as an appealing approach for the realisation of complex thin-walled geometries with architectured porosity. The designed porous structures have promising characteristics since they exhibit a complete three-dimensional geometry whilst maintaining the surface features typical of LPBF depositions. Concurrently to the presence of architectured pores which command the 3D geometry, there is an interest in increasing the surface area of the depositions in order to maximise the active part of the electrodes.

The present investigation hence builds on authors' previous experience in manufacturing Zn-based structures to devise the processing technique for the realisation of complex thin-walled lattice constructions for secondary zinc battery anodes. The work presents the LPBF machine that enables the deposition of structures via SPE alongside with the equipment for the surface characterisation. An experimental design was planned to explore the process feasibility and the effects of processing parameters on the physical characteristics of the as-built electrodes in terms of thickness, surface roughness and strut dimensions. Results indicate that LPBF can be successfully employed to tailor the characteristics of pure Zn thin-walled structures with architectured porosity.

Materials and method

Material

Gas atomised pure zinc powder was employed as feedstock material provided by Linbraze S.r.l. (Sommatino, Italy). The particle size ranged between 15 and 53 μm. The powder was deposited on 1 mm thick zinc substrates.

Table 1. Nominal value of the chemical composition of the zinc powder as declared by the producer

Element	Zn	Pb	Cu	Fe
wt (%)	99.99	<0.003	<0.001	<0.001

Laser Powder Bed Fusion system

To perform the single point exposure deposition of electrodes, a programmable industrial LPBF system was employed (LLA150R, 3DNT, Solbiate, Italy). The machine was adapted with an in-house developed laser scanning system that consisted in a multi-core laser source (nLIGHT, AFX1000, Vancouver, Washington, USA) and a scanner module with integrated focus compensation unit (AM module, Raylase, Wessling, Germany). The laser source emits at 1070 nm and the beam diverging from the core fiber with a 14 µm diameter is collimated with a collimator lens with a focal length of 60 mm. The beam is then focused by a series of transmissive lenses to a beam waist diameter of 70 µm with a Gaussian spatial emission profile. Given the multi-core transport fiber of the laser source, it was also possible to adjust the beam shape from Gaussian to ring-mode. However, for the present research work only the Gaussian profile was employed. In order to coordinate, the laser emission with the scan trajectory, a customised control software was implemented (Direct Machining Control, Vilnius, Lithuania) that allowed to drive the controller card (SP-ICE3, Raylase, Wessling, Germany)[20]. The overall specifications of the LPBF system are reported in Table 2.

Table 2. Specifications of the laser system

Parameter	**Value**
Emission wavelength, λ	1070 nm
Laser max. power, P_{max}	600 W
Core diameter of fiber, d_{f0}	14 µm
Focal length of collimator, f_{col}	60 mm
Beam Parameter Product, *BPP*	0.48
Beam waist diameter, d_0	70 µm

The control software allowed precise control over the temporal emission profile enabling single point exposure scanning strategy. SPE consists in positioning the beam in a stationary manner over the powder bed and exposing the region for a fixed period of time corresponding to a given pulse duration to generate the melting process. Precise coordination of the temporal emission profile with the motion of the galvanometric mirrors of the scanner head required to characterize the laser emission. The temporal profile was characterized by means of a photodiode with a 1 ns rise time sensible at the emission wavelength of the laser beam (DET10A2, Thorlabs, Newton, NJ, USA). The voltage information was converted to power using the average power measured via a power meter (W-3000-D55-SHC, Laserpoint, Vimodrone, Italy). The system was characterized at different levels of pulse duration (t_{on}= 200 – 400 – 800 µs) while keeping a fixed level of emission power (P=50 W), as shown in Figure 1 a. The emission profile was also determined for different levels of power P=50 – 75 – 100 W at a fixed level of pulse duration (t_{on}= 400 µs) as shown in Figure 1 b. It is possible to observe there is a good correspondence between the required emission profile and the emitted level both in terms of pulse duration and emission power. A spike can be noticed in the emission profile immediately after the initial rise time but the laser almost immediately settles to the set level of emission power.

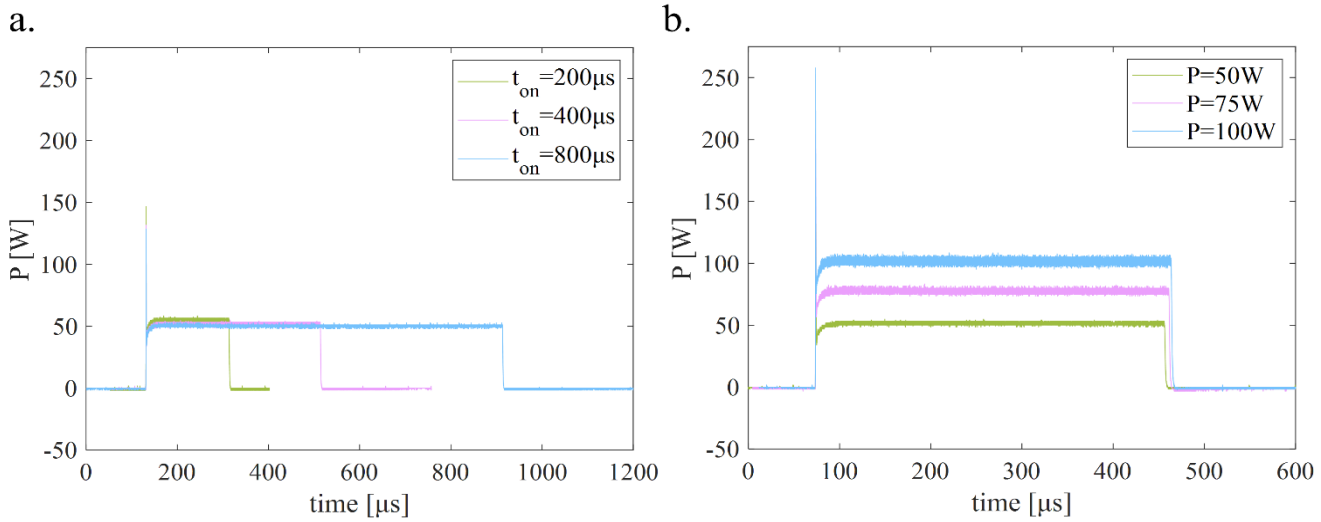

Figure 1. Plot of single pulses at a) fixed level of power P=50W and different levels of pulse duration and b) fixed pulsed duration and different levels of power

Experimental design

An ideal anode material is expected to have high surface area, small sized interconnected pores, with high porosity. Such features are contrasting amongst them. Hence an experimental study was conducted to assess the influence of lattice cell size and process parameters on the geometrical features in view of the battery application requirements. The feasibility of exploiting SPE for the deposition of electrode structures with porous and deterministic surface features was assessed through a full factorial experimental design. A lattice structure with planar development and unit cell geometry, as shown in Figure 2, was employed as base design. The wall length corresponded to l=9 mm whilst the height of the deposition was h=15 mm. A fixed layer thickness of 50 µm was employed and the process was conducted in inert Ar gas atmosphere. The geometry was sliced through the CAM software of the LPBF system. The position of the single point exposure was determined via centroid-based positioning, i.e. in correspondence of the centre-line of the strut geometry (as schematised in Figure 2 b).

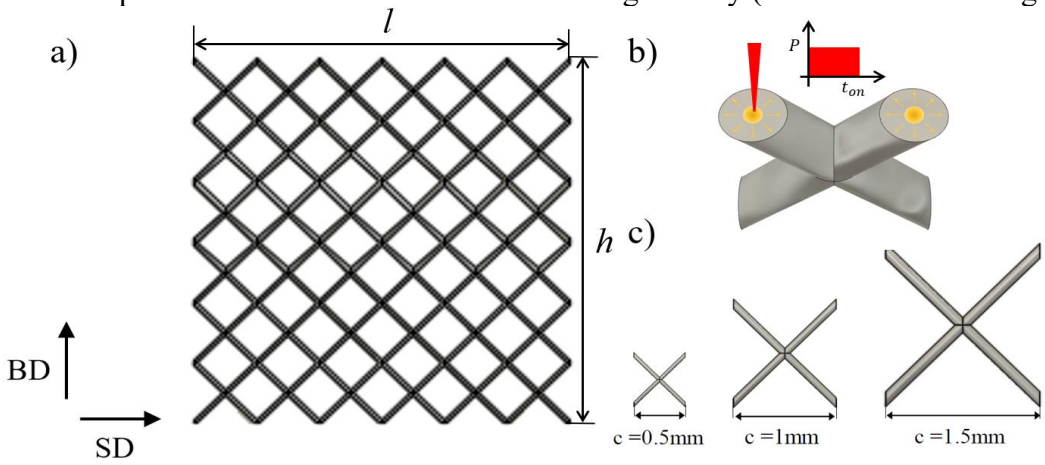

Figure 2. a) Geometry of the lattice structure deposition in terms of height h and length l, b) schematic representation of the Single Point Exposure strategy and c) different unit cell size c=0.5 – 1 – 1.5 mm. BD indicates build direction while SD indicates scan direction

The variable factors of a full factorial experimental design corresponded to three levels of emission power (P=50 – 75 – 100 W) and three levels of pulse duration (t_{on}= 200 – 400 – 800 µs). The unit cell dimension was also taken as a variable factor with three different levels (c= 0.5 – 1 – 1.5 mm), as shown in Figure 2 c. The overall experimental design is reported in Table 3.

Table 3. Fixed and variable factors of the experimental design

Fixed factors	**Value**
Wall length, l (mm)	9
Wall height, h (mm)	15
Layer thickness (µm)	50
Atmosphere	Ar (O_2 <0.3%)
Beam Shape, *BS*	Gaussian (BS0)
Variable factors	**Value**
Power, P (W)	50; 75; 100
Pulse duration, t_{on} (µs)	200; 400; 800
Unit cell dimension, c (mm)	0.5; 1; 1.5

Characterisation equipment

The LPBF process was observed with an external camera positioned laterally to the build plate to observe the process stability in terms of smoke and spatter generation in a qualitative manner. The analysis of the physical characteristics of the LPBF deposited electrodes was conducted by means of macro-photography to demonstrate the process feasibility and via scanning electron Microscope (Zeiss EVO 50, Zeiss, Oberkochen, Germany) to observe in detail the surface characteristics of the depositions. In order evaluate the density of the samples an optical coordinate measurement machine was employed (Mitutoyo Quick Vision ELF QV-202, Mitutoyo, Takatsu-ku, Japan). Samples were illuminated via back-lighting allowing a strong contrast between the anode structure (in black since it was blocking the back-illumination) and empty areas (in white). The density ρ could thus be determined optically with the following relationship calculating the total area of the black pixel (A_{black}) and dividing by the total number of pixels (A_{tot}):

$$\rho = \frac{A_{black}}{A_{tot}} \cdot 100 \tag{1}$$

The surface of the electrodes was digitally reconstructed by means of a focus variation microscope (Alicona Infinite Focus, Graz, Austria). Digital reconstruction allowed to determine the profile roughness (in terms of Ra and Rz) and the Active Area Ratio (AAR) of the electrodes. The AAR is defined as the ratio between the nominal area of the acquisition A_{nom} (which was kept fixed with a region of interest of 3mm by 3mm) and the actual surface area of the electrode available for electron transfer measured $A_{measured}$:

$$AAR = \frac{A_{measured}}{A_{nom}} \tag{2}$$

Results

The first characteristic that can be observed when employing single point exposure to deposit Zn structures is that the vapour-free conditions can be achieved. Figure 3 shows a frame acquired during the deposition process, where the absence of plasma and vapour formation is evident. This is in accordance with previous high speed acquisitions by the authors during the SPE of Zn-0.5Mg, indicating that this scanning approach is adequate to prevent issues that would otherwise be detrimental during the processing of this particular material [21].

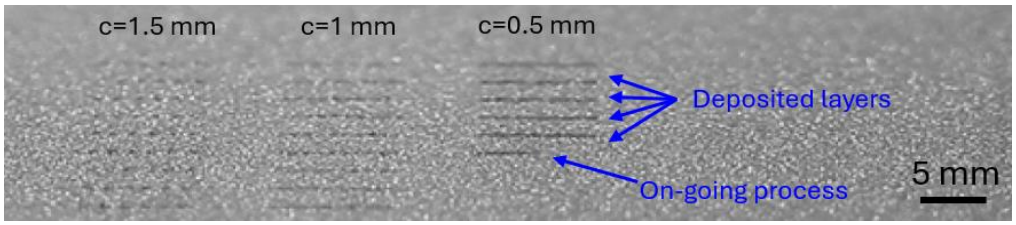

Figure 3. Frame of the ongoing LPBF process showing the vapour free deposition of pure Zn with the SPE strategy.

Representative macrographs of the as-deposited LPBF structures are shown in Figure 4. Fabrication was successful in all the conditions considered in the experimental design. The impact of the imposed unit cell size on the geometrical fidelity can be obeserved. In the case of the larger cells with c=1.5 mm the lattice structure is perfectly defined, whereas with c=0.5 mm the individual struts cannot be precisely discerned.

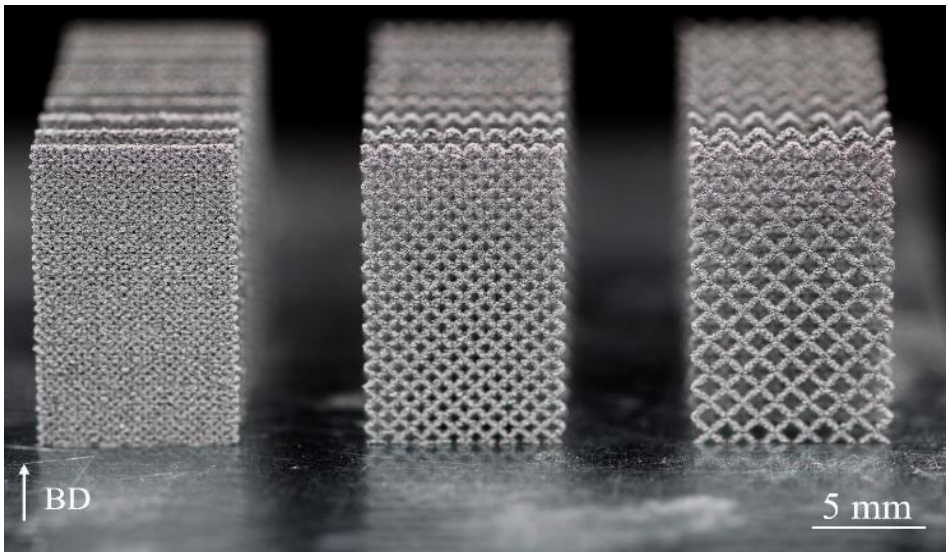

Figure 4. Macro-photograph of the as-deposited pure Zn electrodes with increasing unit cell dimension from left to right c=0.5 – 1 – 1.5 mm. The arrow and symbol BD indicates the Build Direction.

Scanning electron microscopy images in the different conditions are shown in Figure 5, which allow for the assessment of the effect of the process parameters and of the cell geometry. The geometrical effect correlated with the increase in unit cell size corresponds to an increasing amount of open space among the struts. In addition, increases in laser emission power and pulse duration tend to saturate the geometry of the lattice structures, leading towards fully dense depositions.

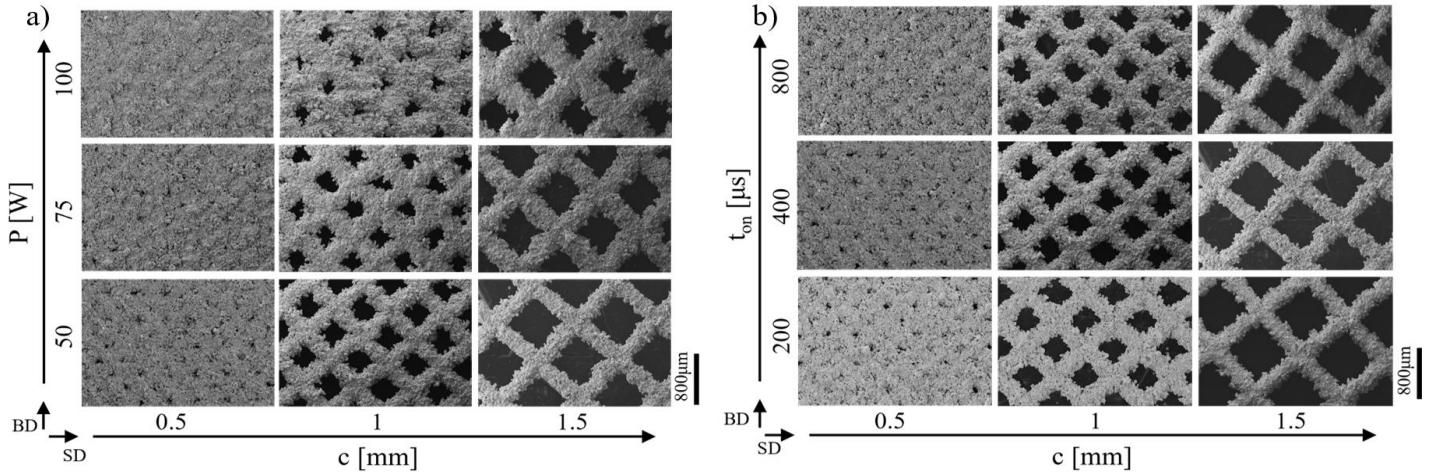

Figure 5. SEM images of the as deposited structures as a function of a) emission power against unit cell size and b) pulse duration against unit cell size. BD and SD indicate the Build and Scanning Directions respectively.

In all cases, it is possible to observe partially molten particles attached to the surface of the depositions. This characteristic is further confirmed by the higher magnification image of the struts shown in Figure 6. In this way, surfaces with an elevated degree of complexity and high surface roughness are obtained. Although structures of this kind generally exhibit poor mechanical properties, their electrochemical activity is enhanced, in principle favouring anodic performance.

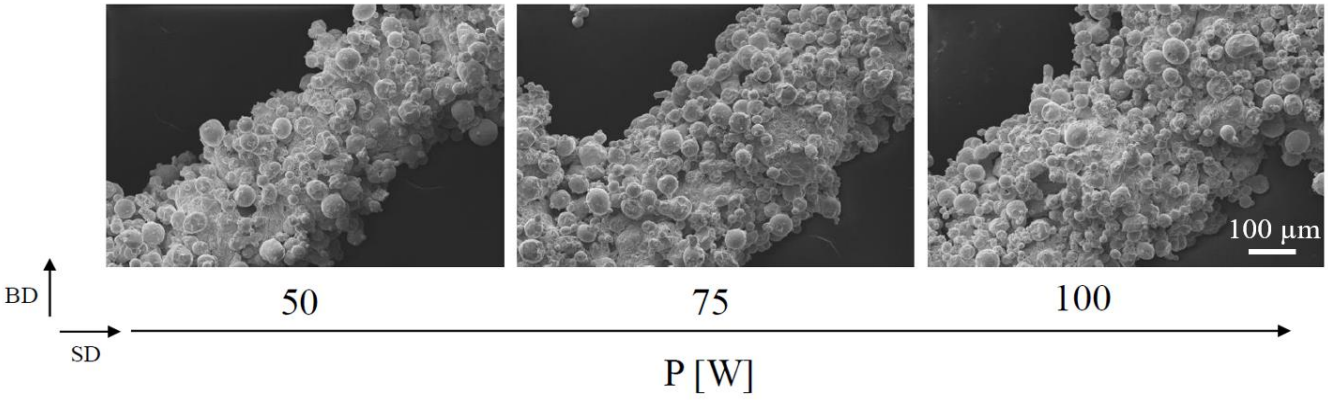

Figure 6. Detailed view of the strut geometry obtained at different levels of emission power. BD and SD indicate the Build and Scanning Directions respectively.

The morphological properties of these materials, roughness in particular, can be effectively quantified through focus variation microscopy. Figure 7 reports surface reconstructions of the strut geometries obtained in this study. We elaborated these datasets to extract average and peak roughness values, and we found that these descriptors are not measurably affected either by the processing conditions or by the strut geometry. Specifically, pooling all the measured data, we estimated an average profile roughness of R_a=19.2 ±0.5 µm, and a peak roughness of R_z= 99.4±1.2 µm, confidence interval indicating one standard deviation. This result highlights that process-independent micro-morphologies can be obtained by SPE-LPBF, while depositing Zn structures via multiple single tracks with continuous wave emission, yielded roughness values that anticorrelate with scan velocity[16].

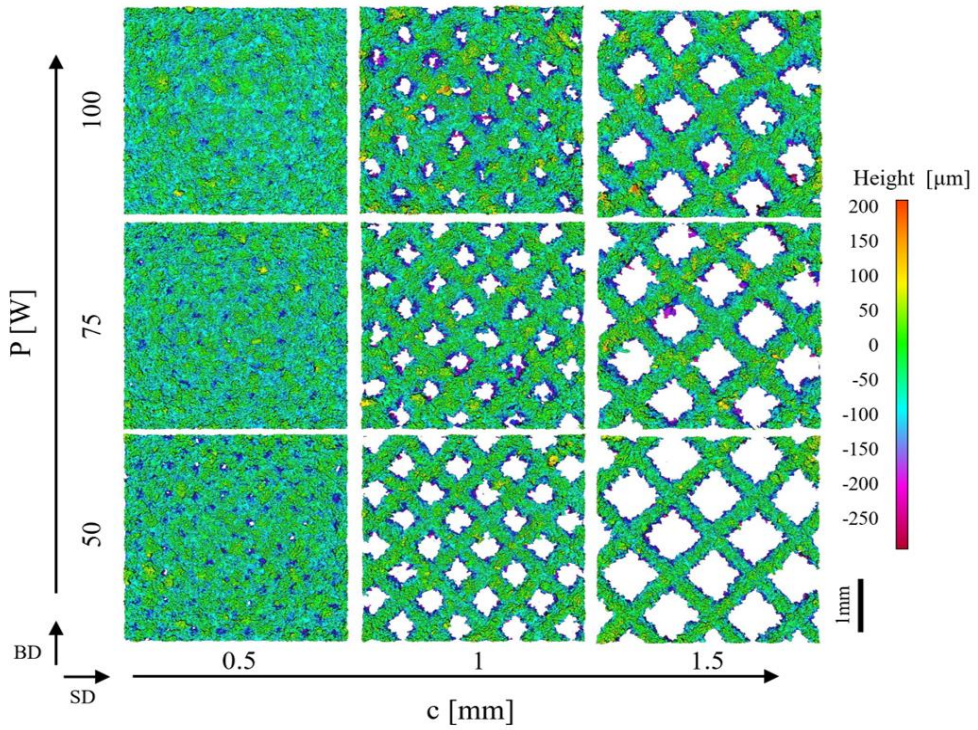

Figure 7. Surface reconstruction obtained via focus variation microscopy for electrodes of different unit cell size, as a function of the emission power

A representative set of optical microscopy acquisitions is reported in Figure 8 a). As previously observed, as the unit cell dimension is reduced, the lattice structure tends towards full density. Increasing the laser emission power also has the effect of reducing the space among struts, thus increasing the optical density of the as-built structures. Corresponding quantitative measurements of the density estimates are reported in Figure 8 b), clearly indicating that the most significantly parameter affecting lattice density is the geometry of the structure. In fact, the lowest density (ca. 50%) is obtained with c=1.5 mm. Moreover, the emission power and pulse duration impact the density of the as-built structures, where more energetic parameters tend to increase the size of the SPE depositions. As a matter of fact, density also appears to be correlated to the strut dimension.

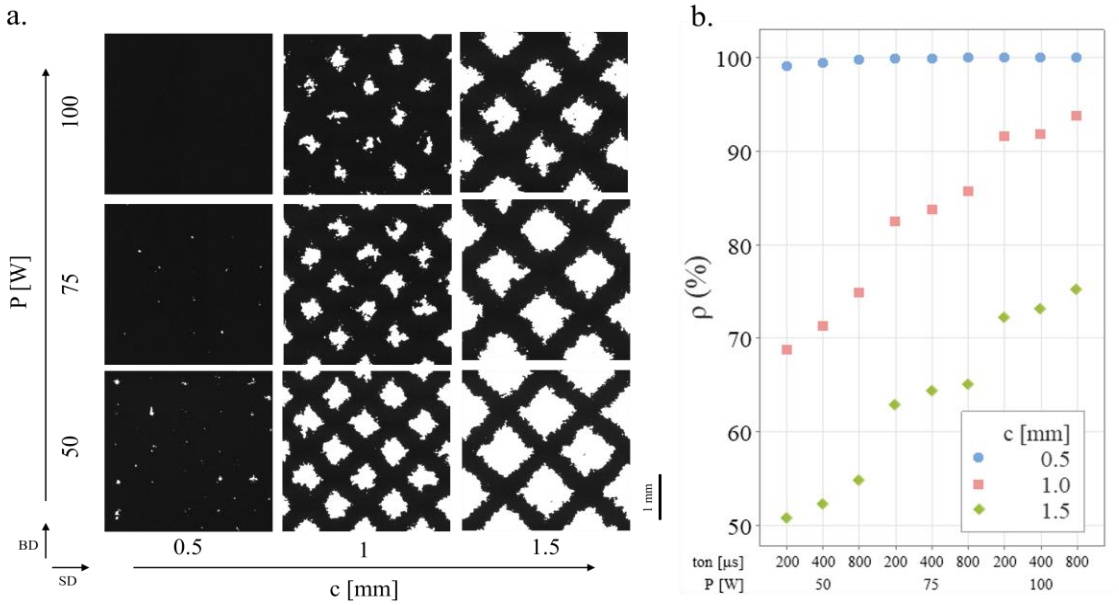

Figure 8. a) Representative back-lighting optical microscopy images of selected Zn structures obtained with the optical coordinate measurement approach and b) optical density measurements, in correspondence of different processing conditions.

In order to characterize the thickness of the electrodes, optical coordinate measurements were performed from a side perspective, as described in Figure 9 a). The results of panel (b) show that the strut geometry does not measurably affect the overall thickness of the electrode, which remains in the range 350-400 µm. It is thus possible to conclude that, on the one hand, the manufacturing parameters do not significantly affect the electrode thickness, and, on the other hand, the obtained thicknesses are compatible with the requirements of batteries with aqueous electrolytes. The thickness can, in any case, be tuned by exploiting smaller beam diameters or powders with reduced particle size as also shown by Regenfuss *et al.* with the micro sintering technology[22].

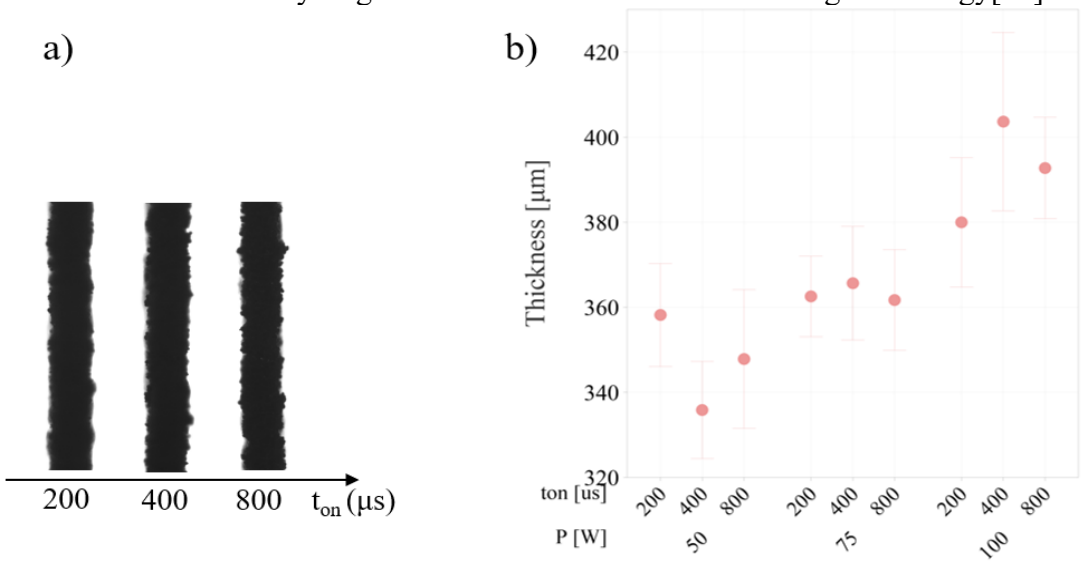

Figure 9. a) Representative side acquisition of the struts for thickness measurement (P=50 W, c=1 mm) and b) thickness of the as-deposited pure Zn electrodes as a function of the process parameters. Error bars correspond to 95% confidence intervals.

The optical microscopy images in Figure 8a also allowed for the estimation of the strut diameter. With the exception of the fully dense c=0.5 mm depositions, for which the strut diameter could not be measured, values were found to be in the range 300-500 µm, larger than the thickness. This discrepancy can be explained with the 45° inclination of the geometry, yielding an ellipsoidal shape, as highlighted in [23]. It can thus be concluded that the single most important parameter controlling the strut diameter is the emission power, whilst the effect of pulse duration tends to saturate. Hence, the relationship established in previous work[21], based on the ablation threshold diameter can be employed also in the present case to estimate the strut diameter.

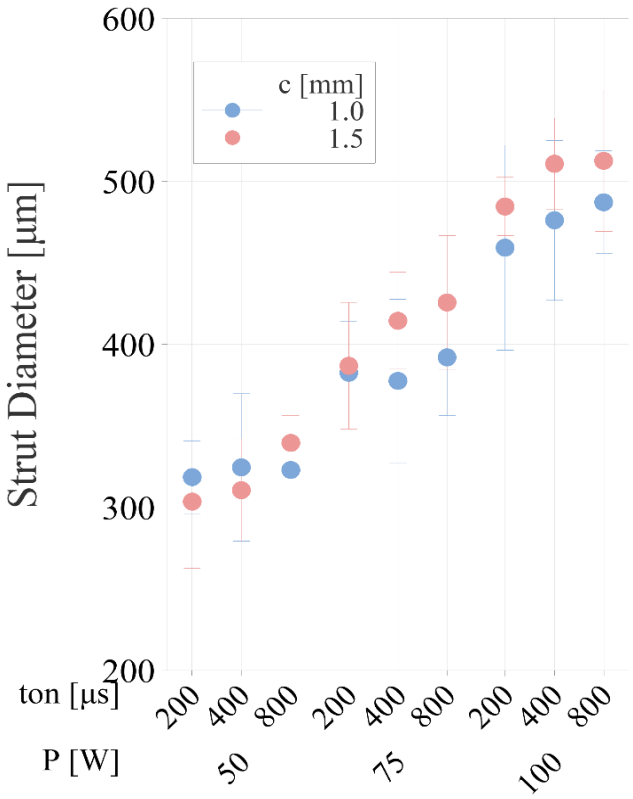

Figure 10. Strut diameter as a function of unit cell size and process parameters. Error bars correspond to 95% confidence intervals.

Finally, the Active Area Ratio (AAR) of the depositions was investigated as a possible estimator factor of the electrochemically active surface area for the electron exchange during battery cycling. The values of this quantity are reported in Figure 11 as a function of process parameters and unit cell size. In this case, it can be observed that the AAR exhibits the highest sensitivity with respect to the unit cell size, while the pulse duration impacts it negligibly. It is worth noting that the highly dense c=0.5 mm deposits, exhibits the highest AAR values found in this research. Instead, if the unit cell size is increased, AAR decreases notably. This result can be explained by the fact that increasing the cell size greatly decreases the inactive space among the struts. Pulse duration has limited effects on AAR, whilst emission power correlates positively with AAR, owing to the impact of this parameter on the strut diameter. In conclusion, in the cases investigated in the present work, the surface complexity is not much affected by the manufacturing parameters, whilst it plays a crucial role in increasing the AAR over the value of 1, characteristic of laminated zinc foil. It is worth noting that, although the AAR is a relevant parameter to determine the active surface of the electrode, with a direct bearing on discharge, it is certainly not the only anode property controlling cycling performance. Shape-change processes occurring during recharge also have to be taken into account.

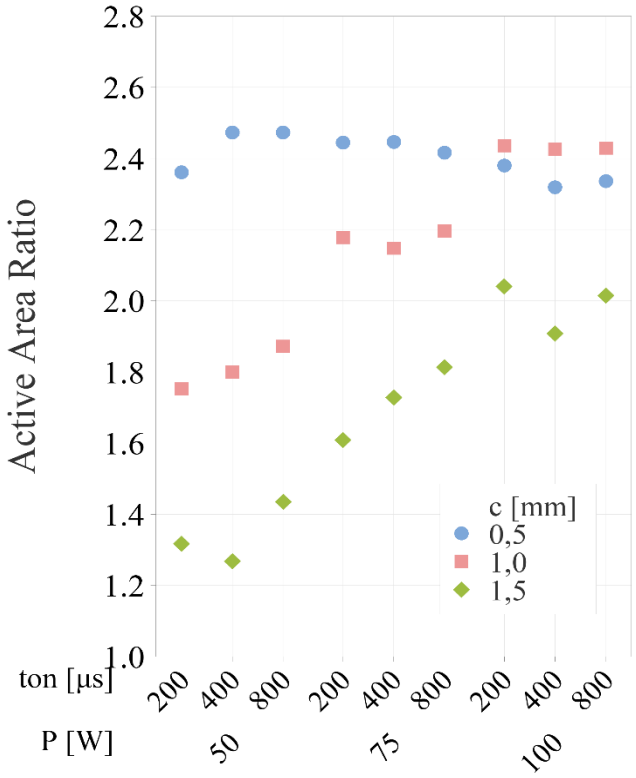

Figure 11. Active Area Ratio (AAR) of the as-built electrodes for different combination of process parameters and unit cell size a) c=0.5 mm, b) c=1 mm and c) c=1.5 mm

Overall, the results indicate that Single Point Exposure LPBF enables the deposition of electrodes with controllable levels of porosity whilst allowing to achieve an increase in terms of the active area up to 2.5 times higher than a flat laminated sheet. From this perspective, electrodes with a unit cell size c=1 mm are most appealing for the final application since they maintain a three-dimensional structure characterized by open porous geometry whilst their Active Area Ratio is in excess of 2.4. On the other hand, electrodes with wider mesh structure (c=1.5 mm) do not allow to achieve values of AAR comparable to those of the fully dense electrodes (c=0.5 mm). The results reported in the present work are thus the starting point for the subsequent research activity regarding the electrochemical characterization of the material performance.

Conclusions and future developments

The results of the present work demonstrate the possibility of depositing binderless Zn anodes with architectured porosity by means of the Laser Powder Bed Fusion process. As-built samples were characterised in terms of the surface characteristics, thickness and density. The depositions currently achieved show promising features in terms of structure, geometry and superficial texture indicating that LPBF is an enabling technique to produce such components. Moreover, the as-built samples demonstrate that the Single Point Exposure strategy may be exploited to tailor the deposition of electrodes allowing control over their density and geometry. Thus, it is possible to exploit the rapid prototyping capabilities of the technology to explore the effects of structures with different density and geometry over the charge-discharge capabilities of pure Zn anodes. Hence, future developments of the present work will be aimed at assessing their electrochemical performance, particularly to understand the impact of manufacturing parameters on the functional electrode performance in secondary zinc battery applications.

Acknowledgments

The authors would like to acknowledge Fondazione Cariplo for funding the research activities via the Amazinc Batt project. The research was supported by nLight and Optoprim that provided the laser source and by Raylase that supplied the scanning head.

References

[1] J. Zhang, X.L. Li, S. Fan, S. Huang, D. Yan, L. Liu, P. Valdivia y Alvarado, H.Y. Yang, 3D-printed functional electrodes towards Zn-Air batteries, Mater Today Energy 16 (2020) 100407. https://doi.org/10.1016/j.mtener.2020.100407.

[2] H. Kabir, K. Munir, C. Wen, Y. Li, Recent research and progress of biodegradable zinc alloys and composites for biomedical applications: Biomechanical and biocorrosion perspectives, Bioact Mater 6 (2021) 836–879. https://doi.org/10.1016/j.bioactmat.2020.09.013.

[3] A. Lahiri, L. Yang, O. Höfft, F. Endres, Biodegradable Zn-ion battery with a lignin composite electrode and bio-ionic liquid based electrolyte: Possible: In situ energy generation by lignin electrocatalysis, Mater Adv 2 (2021) 2676–2683. https://doi.org/10.1039/d0ma00954g.

[4] N. Borchers, S. Clark, B. Horstmann, K. Jayasayee, M. Juel, P. Stevens, Innovative zinc-based batteries, J Power Sources 484 (2021). https://doi.org/10.1016/j.jpowsour.2020.229309.

[5] H. Luo, B. Liu, Z. Yang, Y. Wan, C. Zhong, The Trade-Offs in the Design of Reversible Zinc Anodes for Secondary Alkaline Batteries, Electrochemical Energy Reviews 5 (2022) 187–210. https://doi.org/10.1007/s41918-021-00107-5.

[6] N. Guo, W. Huo, X. Dong, Z. Sun, Y. Lu, X. Wu, L. Dai, L. Wang, H. Lin, H. Liu, H. Liang, Z. He, Q. Zhang, A Review on 3D Zinc Anodes for Zinc Ion Batteries, Small Methods 6 (2022). https://doi.org/10.1002/smtd.202200597.

[7] J.F. Parker, C.N. Chervin, E.S. Nelson, D.R. Rolison, J.W. Long, Wiring zinc in three dimensions re-writes battery performance - Dendrite-free cycling, Energy Environ Sci 7 (2014) 1117–1124. https://doi.org/10.1039/c3ee43754j.

[8] J.F. Parker, C.N. Chervin, I.R. Pala, M. Machler, M.F. Burz, J.W. Long, D.R. Rolison, Rechargeable nickel-3D zinc batteries: An energy-dense, safer alternative to lithium-ion, 2017.

[9] W. Tian, Y. Li, J. Zhou, T. Wang, R. Zhang, J. Cao, M. Luo, N. Li, N. Zhang, H. Gong, J. Zhang, L. Xie, B. Kong, Implantable and biodegradable micro-supercapacitor based on a superassembled three-dimensional network Zn@ppy hybrid electrode, ACS Appl Mater Interfaces 13 (2021) 8285–8293. https://doi.org/10.1021/acsami.0c19740.

[10] T. Maconachie, M. Leary, B. Lozanovski, X. Zhang, M. Qian, O. Faruque, M. Brandt, SLM lattice structures: Properties, performance, applications and challenges, Mater Des 183 (2019) 108137. https://doi.org/10.1016/j.matdes.2019.108137.

[11] R. Cunningham, S.P. Narra, A.D. Rollett, Synchrotron-Based X-ray Microtomography Characterization of the Effect of Processing Variables on Porosity Formation in Laser Power-Bed Additive Manufacturing of Ti-6Al-4V Synchrotron-Based X-Ray Microtomography Characterization of the Effect of Processin, (2017). https://doi.org/10.1007/s11837-016-2234-1.

[12] S. Sanchez, A. Zafari, L. Caprio, A.G. Demir, D. Jafari, Temporal and Spatial Beam Shaping in LPBF for Fine and Porous Ti-Alloy Structures for Regenerative Fuel Cell Applications, Lasers in Manufacturing and Materials Processing 11 (2024) 154–178. https://doi.org/10.1007/s40516-023-00244-3.

[13] A.G. Demir, L. Monguzzi, B. Previtali, Selective laser melting of pure Zn with high density for biodegradable implant manufacturing, Addit Manuf 15 (2017) 20–28. https://doi.org/10.1016/j.addma.2017.03.004.

[14] M. Montani, A.G. Demir, E. Mostaed, M. Vedani, B. Previtali, Processability of pure Zn and pure Fe by SLM for biodegradable metallic implant manufacturing, Rapid Prototyp J 23 (2017) 514–523. https://doi.org/10.1108/RPJ-08-2015-0100.

[15] Y. Chen, P. Wen, M. Voshage, L. Jauer, Y. Qin, J.H. Schleifenbaum, R. Poprawe, Laser additive manufacturing of Zn metal parts for biodegradable implants: Effect of gas flow on evaporation and formation quality, J Laser Appl 31 (2019) 022304. https://doi.org/10.2351/1.5096118.

[16] C. Baldi, L. Caprio, C. Milroy, B. Previtali, A.G. Demir, The Influence of Beam Shape on the Single-Track Formation of Pure Zn Towards the Additive Manufacturing of Battery Electrodes, Lasers in Manufacturing and Materials Processing 11 (2024) 125–142. https://doi.org/10.1007/s40516-023-00237-2.
[17] Y. Li, P. Pavanram, J. Zhou, K. Lietaert, P. Taheri, W. Li, H. San, M.A. Leeflang, J.M.C. Mol, H. Jahr, A.A. Zadpoor, Additively manufactured biodegradable porous zinc, Acta Biomater 101 (2020) 609–623. https://doi.org/10.1016/j.actbio.2019.10.034.
[18] I. Cockerill, Y. Su, S. Sinha, Y.X. Qin, Y. Zheng, M.L. Young, D. Zhu, Porous zinc scaffolds for bone tissue engineering applications: A novel additive manufacturing and casting approach, Materials Science and Engineering C 110 (2020) 110738. https://doi.org/10.1016/j.msec.2020.110738.
[19] Y. Qin, P. Wen, M. Voshage, Y. Chen, P.G. Schückler, L. Jauer, D. Xia, H. Guo, Y. Zheng, J.H. Schleifenbaum, Additive manufacturing of biodegradable Zn-xWE43 porous scaffolds: Formation quality, microstructure and mechanical properties, Mater Des 181 (2019). https://doi.org/10.1016/j.matdes.2019.107937.
[20] F. Guaglione, L. Caprio, B. Previtali, A.G. Demir, Single point exposure LPBF for the production of biodegradable Zn-alloy lattice structures, Addit Manuf 48 (2021). https://doi.org/10.1016/j.addma.2021.102426.
[21] L. Caprio, F. Guaglione, A.G. Demir, Development of Single Point Exposure Strategy to Suppress Vapour Formation During the Laser Powder Bed Fusion of Zinc and Its Alloys, in: Selected Topics in Manufacturing, Springer, 2022: pp. 107–129.
[22] P. Regenfuss, A. Streek, L. Hartwig, S. Klötzer, Th. Brabant, M. Horn, R. Ebert, H. Exner, Principles of laser micro sintering, Rapid Prototyp J 13 (2007) 204–212. https://doi.org/10.1108/13552540710776151.
[23] S. Murchio, M. Dallago, F. Zanini, S. Carmignato, G. Zappini, F. Berto, D. Maniglio, M. Benedetti, Additively manufactured Ti–6Al–4V thin struts via laser powder bed fusion: Effect of building orientation on geometrical accuracy and mechanical properties, J Mech Behav Biomed Mater 119 (2021). https://doi.org/10.1016/j.jmbbm.2021.104495.